Study of an Aeroacoustic Internal Feedback Loop in a High-Speed Jet Using Mode Decomposition Methods

Shota Morita, Aiko Yakeno, Christophe Bogey, Shigeru Obayashi

Study of an Aeroacoustic Internal Feedback Loop in a High-Speed Jet Using Mode Decomposition Methods

Shota Morita*[1,2], Aiko Yakeno[1], Christophe Bogey[3], Shigeru Obayashi[1]

[1]Institute of Fluid Science, Tohoku University, Sendai, Japan
[2]Department of Aerospace Engineering, Tohoku University, Sendai, Japan
[3]CNRS, Ecole Centrale de Lyon, INSA Lyon, Universite Claude Bernard Lyon I, Laboratoire de Mécanique des Fluides et d'Acoustique, UMR 5509, 69130 Ecully, France

*Corresponding author: shota.morita.t7@dc.tohoku.ac.jp (Shota Morita)

Received: January 9, 2024
Revised: March 31, 2024
Accepted: April 25, 2024
Published: August 31, 2024

Abstract

In a subsonic free jet, vortex sound is generated at the end of the potential core, but the mechanism of generation of that sound is still unclear. A recent study proposed that pressure waves propagating upstream in the jets interact with Kelvin–Helmholtz (K–H) instability waves, possibly creating a feedback loop that intensifies (Bogey, 2021). In this study, we applied total a least squares dynamic mode decomposition (TlsDMD) to the time series of the numerical results of an axisymmetric subsonic free jet and performed a detailed analysis of this hypothesis. We extracted the DMD mode at the K–H instability frequency, i.e., the dominant frequency peak near the nozzle exit. The findings indicate that this DMD mode contains not only K–H instability waves but also the pressure waves propagating upstream in the jet. Second, we applied a spatiotemporal Fourier analysis to the DMD mode to describe the characteristics of the pressure waves and confirmed that the pressure waves originate at the end of the jet potential core and that a feedback loop exists at the K–H instability frequency. Our results support this feedback mechanism for sound generation in subsonic free jets.

Keywords

Mode decomposition method, Aeroacoustics, Jet flow, Shear layer instability, Direct Numerical Simulation

1. Introduction

High-speed subsonic jets are fundamental to a variety of fluid machinery, such as jet engines. The Mach number of the exhaust of a jet engine for large airplanes can reach M = 0.9. Since the discovery of Lighthill's eighth power law, considerable work has been carried out to reduce the noise level of exhausts [1]. However, there have been more requests

for noise reduction in large airplanes according to the International Civil Aviation Organization (ICAO) [2]. Therefore, jet noise is still a main research topic in compressible flow. In a high-speed subsonic free jet, noise is considered to be generated by two sources: fine-scale turbulence and large-scale flow structures in the jet potential core [3]. Moreover, the large-scale flow structure in the potential core can form a wave-packet structure. This is an intermittent wave-packet-like structure, which is likely an indirect cause of acoustic waves according to many studies (after Christensen reported the existence of a wave packet in the potential core) [4]. Via direct numerical simulation (DNS) of a high-subsonic free jet, Bogey (2019) confirmed the wave-packet model for subsonic jets and showed that the vorticity at the end of the potential core correlates with the acoustic waves in a far field [5,6]. Alternatively, it was considered that the vortices were generated mainly by the Kelvin–Helmholtz (K–H) instability near the jet exit. These vortices were advected downstream and collapsed into smaller vortices at the end of the potential core. This phenomenon also causes the pressure wave and its interactions to potentially become a noise source. However, the path leading to pressure wave generation in subsonic jets is still under consideration. For instance, Powell [7, 8] suggested that the feedback loop mechanism can facilitate noise generation in impinging jets and supersonic jets. In these cases, K–H instability occurring near the jet exit is encouraged by the acoustic waves originating from the end of the potential core, and an acoustic wave is generated by repeating these fluctuations. In a subsonic free jet, Laufer and Monkewitz (1980) [9] also suggested a kind of feedback loop phenomenon in which the K–H instability wave was stimulated by the wake of small vortices. In more recent studies, Bogey (2021, 2022) [10,11] suggested a feedback loop mechanism between the K–H instability and the pressure wave propagating upstream on a jet axis, which was referred to as the upstream guided jet wave. Their interaction was analyzed by evaluating the autocorrelation of the pressure fluctuations. However, additional detailed investigations are needed from another perspective to support the feedback mechanism.

For several decades, mode decomposition methods have been suggested and applied to clarify sound generation mechanisms. One of the most well-known methods is proper orthogonal decomposition (POD) [12], which is useful for quantitatively determining the underlying mechanism of sound generation. Jordan and Colonius [13] suggested the wave-packet model based on POD analysis. Chavalieli et al. [14] suggested the reduced-order model by using the spectral POD of the wave-packet structure and reported that it agreed well with the frequency response of far-field sound waves. A detailed description of the application of these modal decomposition methods to fluid dynamics analysis was provided by Taira et al.[15]. In addition, a well-known method developed by Schmid [16] in 2010, namely, dynamic mode decomposition (DMD), has attracted increasing attention in terms of flow structure analyses. This method assumes that the flow oscillates in time periodically and obtains a space profile as the basis vector with a certain frequency and growth rate. Compared to POD, DMD can extract both temporal and spatial information separately for unsteady phenomena and is considered to be effective at repairing the coupling of multiple unstable modes. Therefore, in this study, we applied a type of DMD method, referred to as total least squares DMD (TlsDMD) [17], to the numerical database of subsonic free jets at

M = 0.9 by direct numerical simulation (DNS) [5]. It is expected that periodic structures such as K–H instabilities and pressure waves can be extracted. To analyze the pressure wave propagation upstream in more detail, spatiotemporal Fourier analysis of the DMD result was utilized to extract the modes separately depending on their advection direction.

This paper is organized as follows. First, in section 2, we describe the computational conditions of the data used in this study. In section 3, the flow characteristics used in the DMD are represented. In section 4, we show and discuss the DMD results. The results and discussion of the extraction of the feedback loop mechanism by DMD are presented in section 5. Finally, the conclusions of this study are presented in section 6.

2. Methods

2.1. Computational Conditions of the Database for a Subsonic Free Jet of M=0.9

First, the results of the high-fidelity numerical simulations of a subsonic jet obtained by Bogey [5] were investigated. This jet is a three-dimensional and initially disturbed jet, which is the DNS result at a Reynolds number of Re = 3125 and a Mach number of M = 0.9 (hereafter referred to as Re3125FJ). The Reynolds number Re and Mach number M are defined as $\mathrm{Re} = U_j D/\nu$ and $\mathrm{M} = U_j/c_o$, respectively. Here, U_j represents the center of the jet velocity at the jet exit, D represents the diameter of the jet exit, c_o represents the sound speed at an ambient pressure $p_o = 10^5$ [Pa] and temperature $T_o = 293$ [K].

The nozzle-exit conditions of the jet are described in Bogey [5, 6] and briefly listed in **Table 1**. In the DNS, the governing equations are the compressible Navier–Stokes equations written using three-dimensional cylindrical coordinates. They are solved using a numerical framework described and validated in a recent work [18]. Fourth-order 11-point central finite differences were used for the discretization in the spatial direction, and fourth-order 11-point one-sided finite differences were used at the boundaries. For time integration, a Runge–Kutta method was used. In the jet simulation, the jet is excited in the nozzle to obtain a peak turbulent intensity of 1% of the jet mainstream velocity U_j at the nozzle exit. For the DMD analysis, the time width of the snapshots of the flow data was set as $\delta t = 0.076D/U_j$ in all the cases, and the sampling frequency becomes $St_D = fD/U_j = 6.3$.

In this study, sectional pressure time series data in the two-dimensional (z,r) plane at an azimuthal angle $\theta = 0$ were obtained. Here, we define $r/r_0=0$ as the central axis of the jet and $z/r_0=0$ as the jet exit.

Table 1. Computational conditions of the DNS database for the subsonic free jet with M=0.9 [5]

Parameter for the simulation	Re3125FJ
Reynolds number, Re	3125
Mach number, M	0.9
Heat capacity ratio, γ	1.4
Thickness of the Blasius boundary layer profile δ_{BL} at the jet exit	$0.42r_0$ [m]
Turbulence intensity at the nozzle exit	1.0 [%]
Ambient temperature, T_0	293 [K]
Ambient pressure, p_0	10^5 [Pa]

2.2. Total Least Squares Dynamic Mode Decomposition

In this study, TlsDMD [17] was applied to the subsonic free jet to extract the flow structures. In this method, the total least squares method is used for estimating the linear operator **A**. This method can reduce the estimation error compared to the conventional DMD method, which estimates the minimum value problem of the linear operator **A** by the least square method. TlsDMD algorithm is shown below.

We consider snapshot matrices as follows:

$$\mathbf{X} = \{\mathbf{x}_1, \mathbf{x}_2, \ldots, \mathbf{x}_{m-1}\}. \tag{1}$$

$$\mathbf{X}' = \{\mathbf{x}_2, \mathbf{x}_3, \ldots, \mathbf{x}_m\}. \tag{2}$$

Here, $\mathbf{x}_i$ is a column vector including the flow variables (e.g., ϱ, u, v, w, p). Under this condition, DMD is represented by a linear superposition of eigenvectors $\boldsymbol{\phi}_k$, time information at $t = t_i$ as λ_k^i and their amplitudes α_k, called DMD modes, denoted by Eq. (1) as follows:

$$\mathbf{x}_i = \sum_{k=1}^{m} \alpha_k \boldsymbol{\phi}_k \lambda_k^i. \tag{3}$$

The DMD mode $\boldsymbol{\phi}_k$ of Eq. (3) is obtained as the eigenvectors of the linear operator $\mathbf{A}$ of Eq. (4), which is obtained by assuming linear time evolution of the flow:

$$\mathbf{X}' \approx \mathbf{A}\mathbf{X}. \tag{4}$$

Here, $\mathbf{A}$ is obtained by solving the minimum value problem of Eq. (5) using the total least squares method:

$$\arg\min \| \mathbf{X}' - \mathbf{A}\mathbf{X} \|_2^2. \tag{5}$$

In the total least squares method, assume that $\mathbf{X}'$ has an error $\Delta\mathbf{X}'$:

$$\min \left\| \begin{matrix} \Delta\mathbf{X}' \\ \Delta\mathbf{X} \end{matrix} \right\|_2^2, \quad \textit{subject to} \quad \mathbf{X}' + \Delta\mathbf{X}' = \mathbf{A}_{TLS}(\mathbf{X} + \Delta\mathbf{X}) \tag{6}$$

Then, we consider obtaining an approximated linear operator $\mathbf{A}_{TLS}$ via the total least squares method by deriving Eq. (6). We prepare an augmented snapshot matrix, which is defined as Eq. (7):

$$\mathbf{Z} = \left[\mathbf{X} \;\; \mathbf{X}' \right]^T. \tag{7}$$

Next, we perform snapshot POD[19], which is an alternative method to POD, to reduce the data matrix size and to obtain the POD mode $\mathbf{U}_r$ of the time series data $\mathbf{X}$. Then, we construct a reduced dimension matrix of the augmented matrix $\tilde{\mathbf{Z}}$ by using a reduced dimension matrix of $\tilde{\mathbf{X}}$ and $\tilde{\mathbf{X}}'$:

$$\tilde{\mathbf{Z}} = \left[\tilde{\mathbf{X}} \;\; \tilde{\mathbf{X}}' \right]^T = \left[\mathbf{U}_r\mathbf{X} \;\; \mathbf{U}_r\mathbf{X}' \right]. \tag{8}$$

To derive the linear operator $\tilde{\mathbf{A}}$, we perform a singular value decomposition of $\tilde{\mathbf{Z}}$ as shown in Eq. (9):

$$\tilde{\mathbf{Z}} = \tilde{\mathbf{U}}\tilde{\mathbf{S}}\tilde{\mathbf{V}}^* = \begin{bmatrix} \mathbf{U}_{11} & \mathbf{U}_{12} \\ \mathbf{U}_{21} & \mathbf{U}_{22} \end{bmatrix} \begin{bmatrix} \mathbf{S} & \mathbf{0} \\ \mathbf{0} & \mathbf{0} \end{bmatrix} \tilde{\mathbf{V}}^* \tag{9}$$

Here, $\tilde{\mathbf{U}}$ is an orthogonal matrix with a size of $2n*2n$, $\tilde{\mathbf{S}}$ is a diagonal with a size of $2n*m$, and $\tilde{\mathbf{V}}^*$ is a matrix with a size of $m*m$.
By using $\tilde{\mathbf{U}}_{11}$ and $\tilde{\mathbf{U}}_{21}$, $\tilde{\mathbf{A}}$, the approximate value of $\mathbf{A}_{TLS}$ is obtained by the following operation on Eq. (10):

$$\tilde{\mathbf{A}} = \tilde{\mathbf{U}}_{21}\tilde{\mathbf{U}}_{11}^{-1}. \tag{10}$$

By solving the eigenvalue problem for $\tilde{\mathbf{A}}$, we obtain the DMD mode in TlsDMD $\boldsymbol{\phi}_k$ and its corresponding eigenvalue λ_k. From the eigenvalue λ_k, the growth rate σ and frequency St_D of the DMD mode $\boldsymbol{\phi}_k$ can be obtained as in Eq. (11).

$$\sigma = \frac{ln\|\lambda\|}{\Delta t}, St_D = \frac{Arg(\lambda)}{2\pi\Delta t}. \tag{11}$$

From Eq (10), we can obtain the DMD modes. We can also visualize the time evolution of the DMD mode, and let $\mathbf{f}(k\Delta t)$ be the time evolution of the DMD mode, which can be obtained by the following Eq. (12):

$$\mathbf{f}(k\Delta t) = \boldsymbol{\phi}\lambda^k. \tag{12}$$

In this study, we use this equation to compute and evaluate the temporal evolution of pressure waves in DMD modes. In this study, in-house solver was used to perform the TlsDMD.

2.3. DMD Mode Selection

DMD has the potential to explain the flow characteristics of periodic structures by extracting the mode in a complex flow. One of the most commonly used methods is the compressed sensing method, based on the amplitude of the DMD mode α_k, by Jovanovic et al. [20]. However, although it has the largest energy among the modes, the DMD mode is sometimes not the key structure causing flow phenomena. For this reason, several mode selection methods have been proposed for DMD analyses. In this study, we apply frequency analysis for a selection of DMD modes, and we extract the DMD modes that are more directly related to the flow field based on the obtained peak frequencies. Moreover, the amplitude of the DMD mode is also examined to verify that the DMD mode has physical meaning in the flow field in terms of energy. Then, if more than one corresponding DMD mode is extracted, then the mode with the largest amplitude is used for visualization.

3. Results and Discussion on Flow Characteristics of the Jet

In this section, we show the results of the Reynolds stress and frequency analysis computed from the time series data of the two simulation cases. From these results, we discuss the transition position of turbulence and the frequency peak of pressure fluctuations. Based on parameters, the region where the DMD is applied and the frequency extracted by the DMD will be determined.

3.1. Reynolds Stress Around the Potential Core

To determine the region in which tlsDMD is performed, we examine the Reynolds stress distribution, $\overline{u'_z u'_r}$, around a potential core, as shown in **Figure 1**. The contour shows

the strength of the Reynolds stress $\overline{u'_z u'_r}$; the vertical axis is the coordinate r in the direction of the jet axis, and the horizontal axis is the coordinate z in the direction of the jet axis. From **Figure 1**, the peak of the Reynolds stress is located near z/r_0=15. This peak indicates the position of the end of the potential core, and the wake transitions to turbulence are generated from this position. Therefore, to investigate the relationship between the pressure waves generated at the end of the potential core, TlsDMD is applied to the region from the jet exit to the end of the potential core, where $0 < z/r_0 < 18$ and $0 < r/r_0 < 3$.

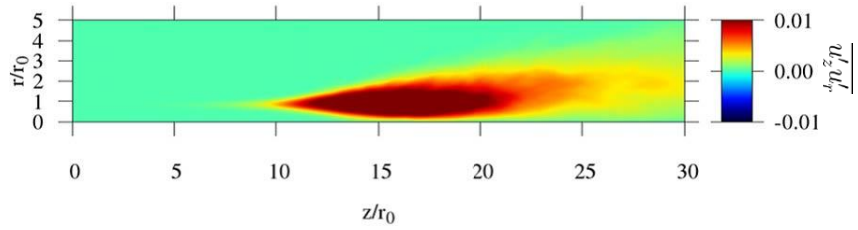

Figure 1. The spatial distribution of the Reynolds stress $\overline{u'_z u'_r}$. The contour ranges from -0.01 to 0.01, from blue to green to red.

3.2. Frequency Analysis Results from Near to Far Flow Field

To understand the behavior of a pressure wave in a free jet, a frequency analysis was performed on each time series data for Re3125FJ, and the results are shown in **Figure 2**. In this figure, the vertical axis shows the Power Spectra Density (PSD) of the signal and the horizontal axis shows the Strauhal number $St_D=fD/U_j$. Here, f is the time frequency of the signal. The results indicate that the frequency peaks change as the position moves downstream. First, near z/r_0=0.0, the frequency peak at St_D=0.47 is dominant. Furthermore, up to z/r_0=6.0, there are some frequency peaks in the high-frequency region as subharmonics with a frequency of St_D=0.47. These peaks are considered to be guided jet waves, which are found in the free jet on the jet axis. As shown in **Figure 2**, the peaks at St_D=0.47 were dominant all the way to the end of the potential core. A broad frequency peak is observed at the end of the potential core. This peak indicates the superposition of pressure fluctuations due to vortex generation at various scales at the same position.

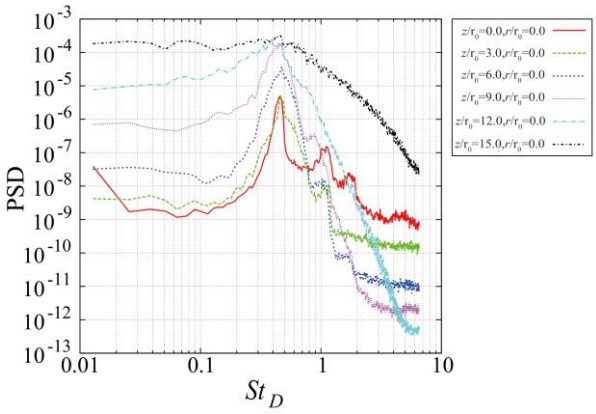

Figure 2. Frequency analysis results of the pressure fluctuation of the free jet in the near-far-field direction.

Next, to examine the behavior of the pressure fluctuation near the jet exit, frequency analyses at (z/r_0, r/r_0) = (0.0, 0.0), (0.0, 0.2), (0.0, 0.8), and (0.0, 1.0) were performed for Re3125FJ. The results are shown in **Figure 3**. First, the peak at St_D=0.47 is dominant at all locations near the jet exit. This value is close to that of the theoretical and experimental solutions of the K–H instability [21] (details are described in the next section). Therefore, St_D=0.47 is considered to be the frequency at which the K–H instability is induced. Other frequency peaks, St_D=0.77, St_D=1.15, and St_D=1.4, are obtained.

From these results, the DMD mode corresponding to the frequency peaks were extracted. Therefore, for Re3125FJ, four DMD modes with St_D=0.47, St_D=0.77, St_D=1.15 and St_D=1.4 are extracted.

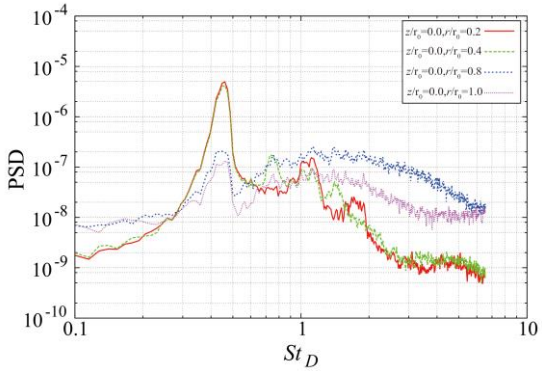

Figure 3. Frequency analysis results of the pressure fluctuation near the jet exit of Re3125FJ.

3.3. K–H Instability Frequency Near the Jet Exit

In this section, the most dominant frequency peak near the jet exit, St_D=0.47, for Re3125FJ is examined and discussed in relation to the flow structure of the flow field. Here, St_D is the Strauhal number scaled by the diameter of the jet exit D. We considered the appearance of a regular structure with pressure fluctuations as a vortex caused by a K–H instability.

The frequency at which this K–H instability is induced is known from linear stability theory [21] and from various experiments using jets [22]. It is reported that his frequency can be found by a certain range of Strouhal number scaled by the initial momentum thickness near the jet exit [23], θ_0 as follows:

$$St_\theta = \frac{f\theta_0}{U_j} \approx 0.009 - 0.018 \tag{13}$$

where U_j is the central flow velocity at the jet exit and f is the time frequency of the signal. The momentum thickness, θ_0, can be calculated using Eq. (14).

$$\theta_0 = \frac{1}{U_j{}^2} \int_0^{r_0} \bar{u}\left(U_j - \overline{u(0)}\right) dz. \tag{14}$$

Here, r_0 is the jet radius, and $\bar{u}$ is the time-averaged velocity in the flow direction.

According to the present numerical simulation data, the momentum thickness θ_0 is $\theta_0 = 0.05r_0$ for Re3125FJ. Therefore, the K–H instability frequency in each case must be at least in the range of $St_D = 0.36 - 0.72$ for Re3125FJ when θ_0 is converted to diameter based Strouhal number. Compared to the frequency peaks in **Figure 3**, the K–H instability frequency for Re3125FJ is considered to be $St_D = 0.47$.

4. Visualization Results of Dynamic Mode Decomposition

In this section, TlsDMD is applied to the time series data of pressure fluctuations in Re3125FJ, and the DMD modes corresponding to the frequency peaks derived from the frequency analysis results described in the previous section are extracted and visualized.

4.1. Eigenvalue Distribution of DMD Modes

The relationship between the amplification factor σ and the frequency St_D of each DMD mode calculated from the eigenvalues of the DMD modes is shown in **Figure 4**. The horizontal axis shows the frequency of each DMD mode, and the vertical axis shows the amplification factor. The red dots are the relationships between the frequency and amplification factor of each DMD mode. The green points are the DMD modes corresponding to St_D = 0.47, 0.77, 1.15, and 1.4 for Re3125FJ. **Figure 4** shows that there is one DMD mode that corresponds to each of the frequency peaks. The four DMD modes corresponding to the frequency peaks have an amplification factor close to zero, and we can conclude that the structure oscillates periodically in time.

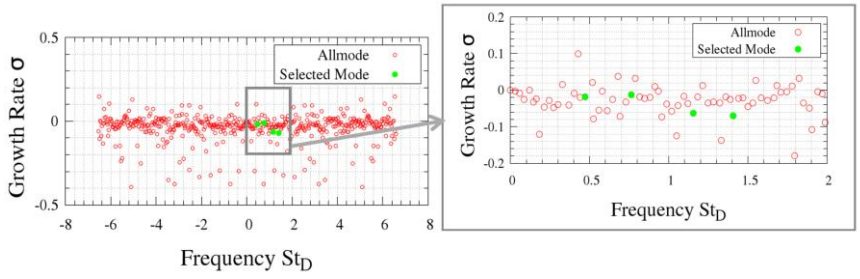

Figure 4. Relationship between growth rate and frequency for each DMD mode for Re3125FJ.

Next, to investigate how energetic the chosen mode is, the amplification of the DMD mode α is computed from the inverse of Eq. (3). The results are shown in **Figure 5**. From this result, the DMD mode, which has St_D = 0, which means time-averaged flow, has an amplitude of α = 6. On the other hand, the amplitude of the selected modes, which are colored green, is approximately α = 0.1. If the growth rate is close to zero, then the amplitude of the DMD mode is considered to be the order of the energy in the original flow data. Taking the energy of the time-averaged flow as 1, these DMD modes are approximately 0.017. Since the maximum pressure fluctuation in the jets used in this study is approximately 0.1 with respect to pressure, these DMD modes are not relatively large but are physically meaningful. Therefore, these selected DMD modes are discussed in this study.

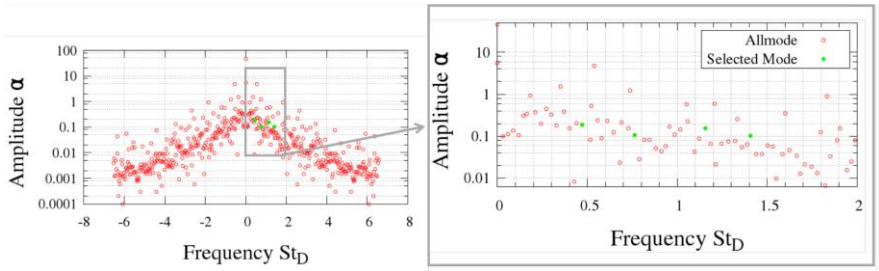

Figure 5. Relationship between the amplitude and frequency for each DMD mode. Red points: All DMD modes. Green points: DMD modes selected in this study.

4.2. Visualization Results of the DMD Modes

To investigate the flow structures of the extracted DMD modes, the visualization results of the four extracted DMD modes are shown in **Figure 6** (a)-(d). The contour of these figures show the signal strength of DMD mode, which is formulated by Eq. (12). Since these values are DMD modes of pressure fluctuations, they can be considered as the spatial structure of pressure fluctuations oscillating at a certain frequency. Based on this, the following discussion is described.

In all the DMD modes (a)-(d), periodic pressure fluctuations propagating at r/r_0=0.9 above the shear layer can be observed. However, in (c) and (d), pressure fluctuations are observed near the jet exit and around z/r_0=15. The pressure fluctuations in (c) and (d) correspond to the sound waves at the nozzle lip near the jet exit and the turbulence near the end of the potential core. From the DMD mode of **Figure 6** (a) for St_D = 0.47, we can see that the vortex due to the K–H instability appears on the shear layer at r/r_0=0.9 and transitions to turbulence in the wake. In addition, a unique phenomenon in the DMD mode (**Figure 6 (a)**) is that pressure waves are generated on the jet axis. To confirm the propagation direction of the pressure wave, the dispersion relation at r/r_0=0 in each selected DMD mode is shown in **Figure 7**(a), (b), (c), and (d). The horizontal axis shows the spatial wavenumber of the jet flow direction k, and the vertical axis shows the time frequency St_D. Here, if it has a positive wavenumber in frequency space, it means that the original data has waves propagating in the positive direction. In other words, here it is a wave propagating in the

downstream direction of the jet. If the wavenumber is negative, it means the vice versa. To divide the wavelength into frequency, we can determine the phase speed of the wave. Therefore, in these figures, if the peak is found in the range of negative wavenumber, then the wave that propagates in the upstream direction exists in the data. Alternatively, if the peak falls within the positive wavelength range, then vice versa. From these graphs, two peaks at negative and positive wavelengths were found in DMD mode for (a) St_D = 0.47, (b) St_D = 1.15 and (d) St_D = 1.4, which indicates that the pressure wave on the jet axis propagates upstream in addition to the pressure wave propagating downstream. This means that the pressure wave on the jet axis propagates upstream and is considered to be the guided jet wave where the upstream wave propagates around the axis center at the end of the potential core. However, this wave propagating to the upstream wave at $r/r_0 = 0$ is noisy due to turbulence and can be identified only up to z/r_0=3.0 in the DMD mode. To identify the location where this wave is generated, structure extraction is performed using spatio-temporal Fourier analysis, as described in the next section.

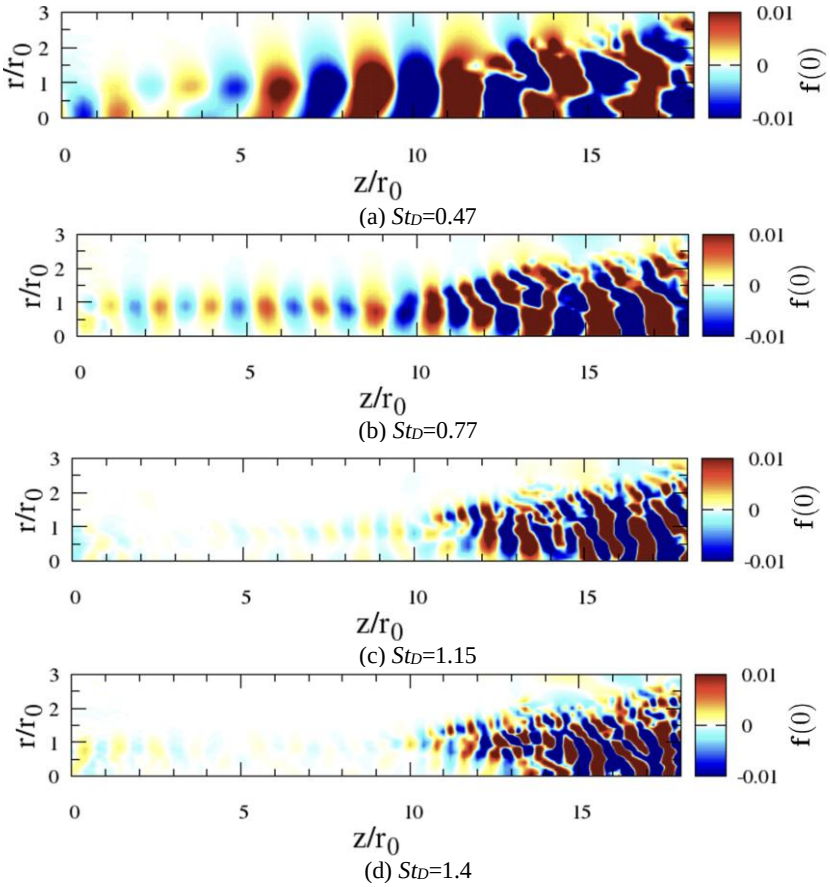

(a) St_D=0.47

(b) St_D=0.77

(c) St_D=1.15

(d) St_D=1.4

Figure 6. Visualization results of DMD modes corresponding to frequency peaks. The contour shows $\mathbf{f}(k\Delta t) = \boldsymbol{\phi}\lambda^k$, which is formulated by Eq. (12).

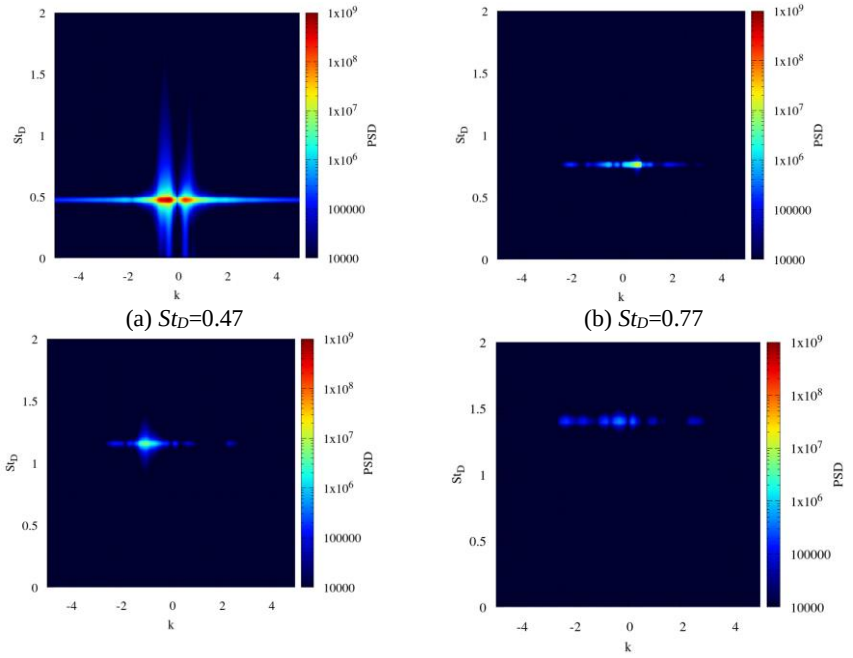

(a) St_D=0.47 (b) St_D=0.77

(c) St_D=1.15 (d) St_D=1.4

Figure 7. Dispersion relation of DMD modes at the jet axis (r=0). The data are used for frequency analysis in the range of z/r_0 = 0.0 to z/r_0 = 6.0 on the jet axis. Vertical axis shows Strouhal number of the pressure signal and Horizontal axis shows the wavenumber of the jet direction.

5. Further Investigation of the DMD Results

5.1. Extraction of Waves Propagating Upstream via Spatiotemporal Fourier Analysis

In the previous section, waves propagating upstream were found at St_D = 0.47, which is the most dominant among the DMD results and induces K–H instability. However, upstream waves were not observed because the turbulence became stronger near the end of the potential core, and it was unclear where the waves originated. Therefore, we attempted to extract only these upstream waves by applying spatiotemporal Fourier analysis to the time evolution data of the DMD mode at St_D = 0.47. An explanation of the method is given below. First, let $f(z,r,t)$ be the time series data of the time evolution of DMD modes; and this frequency space is represented as follows:

$$f(z,r,t) = \sum_{j=-\infty}^{\infty} \sum_{k=-\infty}^{\infty} \sum_{l=-\infty}^{\infty} F_{jkl} exp[i2\pi(k_j x + k_k r + k_l t)]. \tag{15}$$

Here, k_j is the wavenumber in space in the z-direction (jet axis direction), k_k is the wavenumber in the r-direction (radial direction), and k_l is the wavenumber in the time direction (time frequency). $F_{jkl} = F(k_j, k_k, k_l)$ is the amplitude of waves with these wavenumbers.

$$k_j = \frac{j}{L_z}, k_k = \frac{k}{L_r}, k_l = \frac{l}{T}. \tag{16}$$

In this case, we set the filter function $M(j, k, l)$ under the following conditions.

$$M(j,k,l) = \begin{cases} 1 \ (if \ k_j < 0) \\ 0 \ (if \ k_j > 0) \end{cases} . \tag{17}$$

Using the above filter functions, the time evolution $f(z,r,t)$ of the DMD mode can be reconstructed by extracting only the frequency components of the negative wavenumber k_j, as shown in Eq. (18):

$$\tilde{f}(z,r,t) = M(j,k,l) \sum_{j=-\infty}^{\infty} \sum_{k=-\infty}^{\infty} \sum_{l=-\infty}^{\infty} F_{jkl} exp[i2\pi(k_j x + k_k r + k_l t)]. \tag{18}$$

Figure 8 shows the extraction results of the time evolution of DMD modes at St_D = 0.47 using Eq.(17) and Eq. (18). The results indicate that in the DMD mode at St_D = 0.47, the waves propagating upstream are emitted from approximately z/r_0 = 15, which corresponds to the position of the end of the potential core, although the noise is large. Since jet noise is generated from the end of the potential core, this result suggests that the pressure wave propagating upstream is a sound wave generated at the end of the potential core.

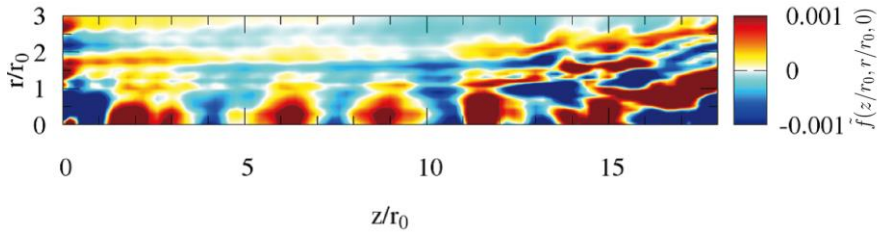

Figure 8. The extraction results of the time evolution of DMD modes at St_D = 0.47 by using spatiotemporal Fourier analysis which is formulated by Eq. (17) and (18).

5.2. Acoustic Impedance

Using the concept of acoustic impedance, in this section, the reason why upstream-propagating waves are reflected at the end of the potential core is discussed. Acoustic impedance is an analogy that explains the ease of sound propagation between different media using the concept of impedance in electromagnetism [24]. By applying this index to the numerical results in this study, the behavior of sound waves at the end of a potential core is examined. An overview of the acoustic impedance is given below. When a sound pressure of p_i and a particle velocity of u_i are incident between different media, as shown in **Figure 9**, we consider a problem where the sound pressure of the transmitted wave is p_t, the wave velocity is u_t, the sound pressure of the reflected wave is p_{ref} and the wave velocity is u_{ref}. In this case, the acoustic impedance can be expressed as follows:

$$z_1 = p_i/u_i = p_{ref}/u_{ref}, z_2 = p_t/u_t. \tag{19}$$

When this incident wave is a plane wave, Eq. (19) can be rewritten as Eq. (20):

$$z_1 = \rho_i c_i. \tag{20}$$

In this case, we define the local acoustic impedance at a certain point z_l and calculate it via the following equation:

$$z_l = \rho_i c_i. \tag{21}$$

From the Newton–Laplace equation, using the aeroelastic modulus of air K and the density ρ, the speed of sound c_0 can be rewritten as follows:

$$\sqrt{K/\rho} = c_0. \tag{22}$$

When K is assumed to be adiabatic, $K = \gamma P$, where γ is the heat capacity ratio. Therefore, γP can be substituted into Eq. (22), and Eq. (21) can be rewritten as follows:

$$z_l = \sqrt{\rho_i p_i \gamma}. \tag{23}$$

In this case, the acoustic impedance is given by if we calculate the acoustic impedance using the turbulence component of the pressure component, we obtain the following equation.

$$z_l = \sqrt{\rho_i \frac{1}{2}\rho(u'^2 + v'^2 + w'^2)}. \tag{24}$$

By applying Eq. (24) to the free jet calculation results for Re3125FJ in this study, a snapshot of the acoustic impedance can be obtained, as shown in **Figure 9**. The acoustic impedance of this jet increases around $z/r_0 = 15$ on the jet axis, which is the end of the potential core of a jet. The sound waves generated by the end of the potential core can be explained by the local increase in acoustic impedance.

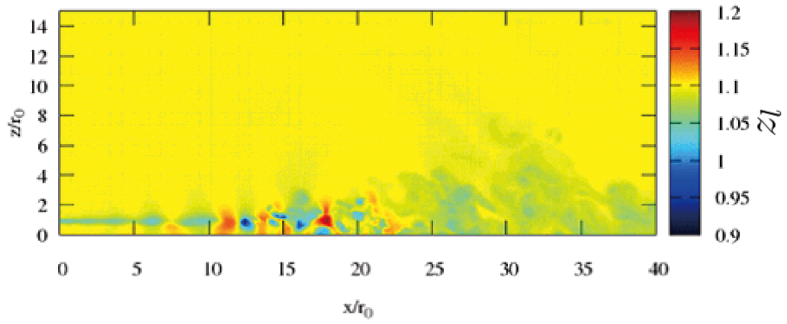

Figure 9. Visualization results of instantaneous values of acoustic impedance z_l formulated by Eq. (24).

6. Conclusion

To investigate the feedback loop phenomenon in subsonic jets suggested by recent studies, total least squares dynamic mode decomposition (TlsDMD), a type of DMD, was applied to high-fidelity free jet numerical simulation data obtained by Bogey (2019). First, a frequency analysis was performed for the pressure fluctuations in the region near the jet exit in the numerical results. As a result, dominant frequency peaks were obtained at $St_D = 0.47$, 0.77, 1.15, and 1.4 for a free jet with Re = 3125. The frequency peaks at $St_D = 0.47$ for the free jet with Re = 3125 were found to be the frequencies that induced the K–H instability. Next, we applied TlsDMD to the time series data of pressure fluctuations in the potential core in these jet data. In addition, the DMD modes corresponding to the frequency peaks were extracted from the DMD results, and the following results were obtained. At $St_D = 0.47$, which is the frequency that induces K–H instability, pressure fluctuations due to K–H instability in the shear layer at $r/r_0 = 0.9$ and waves propagating upstream on the jet axis at $r/r_0 = 0$ were observed. These upstream propagating pressure waves are considered to be

guided jet waves. The observation results of the DMD mode at $St_D = 0.47$ suggest that the guided jet waves can affect the K–H instability. This result supports the concept of the feedback loop phenomenon in subsonic jets; however, the origin of these pressure waves could not be found because of turbulence in the downstream region. To investigate the origin of the pressure waves propagating in the upstream direction on the jet axis, spatio-temporal Fourier analysis was applied to the time series data of the DMD mode at $St_D = 0.47$. This result showed that the upstream wave was generated from the end of the potential core. This indicates that the pressure wave propagating upstream is a sound wave generated from the end of the potential core. The cause of the upstream propagation of the sound wave was discussed using the concept of acoustic impedance of plane wave reflection. As a result, it was found that the acoustic impedance increases at the transition point to turbulence at the end of the potential core in the case of free jet flow. This finding suggests that the temporary increase in dynamic pressure due to turbulence may reflect the sound waves and propagate them upstream. However, we only deal with low Reynolds number case, and there are differences in Reynolds numbers in cases such as jet engines. As a future work, it is necessary to investigate whether the feedback mechanism occurs in Higher Reynolds number case by using the same method.

CRediT Authorship Contribution Statement

Shota Morita: Conceptualization, Methodology, Software, Formal analysis, Writing – Original draft, Writing – review & editing. Aiko Yakeno: Conceptualization, Methodology, Formal analysis, Writing – review & editing. Christophe Bogey: Conceptualization, Methodology, Resources, Writing – review & editing, Shigeru Obayashi: Conceptualization, Methodology, Writing – review & editing.

Declaration of Competing Interests

The authors declare that they have no known competing financial interests or personal relationships that could have appeared to influence the work reported in this paper.

Acknowledgments

This work was supported by the JSPS Core-to-Core Program (grant number: JPJSCCA20210005), JST SPRING (grant number: JPMJSP2114) and ELyT collaboration research between École Centrale de Lyon (France) and Tohoku University (Japan).

All of mode decomposition methods and analysis methods were performed on the supercomputer system “AFI-NITY” at the Advanced Fluid Information Research Center, Institute of Fluid Science, Tohoku University.

The jet was simulated using the HPC resources of PMCS2I of Ecole Centrale de Lyon and of IDRIS under the allocation 2020-2a0204 made by GENCI (Grand Equipement National de Calcul Intensif).

References

[1] Lighthill, M.J. (1952) On Sound Generated Aerodynamically I. General Theory, *Proceedings of the Royal Society of London.* , **211,** 564–587. https://doi.org/10.1098/rspa.1952.0060

[2] Dickson, N. (2013) ICAO Noise Standards, *ICAO Symposium on Aviation and Climate Change*, https://www.icao.int/Meetings/Green/Documents/day%201pdf/session%202/2-Dickson.pdf

[3] Tam, C.K., Viswanathan, K., Ahuja, K., Panda, J. (2008) The Sources of Jet Noise: Experimental Evidence, *Journal of Fluid Mechanics.*, **615**, 253. https://doi.org/10.1017/S0022112008003704

[4] Mollo-Christensen, E.L (1967) Jet Noise and Shear Flow Instability Seen from an Experimenter's Viewpoint, *Proceedings of the Royal Society of London.* , **34,** 1. https://doi.org/10.1115/1.3607624

[5] Bogey, C. (2019) Two-dimensional Features of Correlations in the Flow and near Pressure Fields of Mach Number 0.9 Jets, AIAA Scitech 2019 Forum, 2019-0806. https://doi.org/10.2514/6.2019-0806

[6] Camussi, R., Bogey, C. (2021) Intermittent Statistics of the 0-mode Pressure Fluctuations in the Near Field of Mach 0.9 Circular Jets at Low and High Reynolds Numbers,Theoretical Computational. Fluid Dynamics, 35(2), 229-247. https://doi.org/10.1007/s00162-020-00553-9

[7] Powell, A. (1961) On the Edgetone, *The Journal of the Acoustical Society of America.*, **33,** 395. https://doi.org/10.1121/1.1908677

[8] Powell, A. (1953) The Noise of Choked Jets, *The Journal of the Acoustical Society of America.*, **25,** 385. https://doi.org/10.1121/1.1907052

[9] Laufer, J., Monkewitz, P. (1980) On Turbulent Jet Flows - A New Perspective, 6th Aeroacoustics Conference , 1980-962. https://doi.org/10.2514/6.1980-962

[10] Bogey, C. (2021) Acoustic Tones in the Near-Nozzle Region of Jets: Characteristics and Variations between Mach Numbers 0.5 and 2, *Journal of Fluid Mechanics.*, **921**, A3. https://doi.org/10.1017/jfm.2021.426

[11] Bogey, C. (2022) Interactions between Upstream-propagating Guided Jet Waves and Shear-layer Instability Waves near the Nozzle of Subsonic and Nearly Ideally Expanded Supersonic Free Jets with Laminar Boundary Layers, *Journal of Fluid Mechanics*, 949, A41. https://doi.org/10.1017/jfm.2022.776

[12] Berkooz, G., Holmes, P., Lumley, J. (2003) The Proper Orthogonal Decomposition in the Analysis of Turbulent Flows, *Annual Review of Fluid Mechanics*, **25,** 539. https://doi.org/10.1146/annurev.fl.25.010193.002543

[13] Jordan, P., Colonius, T. (2013) Wave Packets and Turbulent Jet Noise, *Annual review of fluid mechanics*, **45,** 173. https://doi.org/10.1146/annurev-fluid-011212-140756

[14] Cavalieri, A.V.G., Jordan, P., Lesshafft, L. (2019) Wave-Packet Models for Jet Dynamics and Sound Radiation, *Applied Mechanics Reviews*, **71,** 020802. https://doi.org/10.1115/1.4042736

[15] Taira, K., Brunton, S.L., Dawson, S.T., Rowley, C.W., Colonius, T., McKeon, B.J., Schmidt, O.T., Gordeyev, S., Theofilis, V., Ukeiley, L.S. (2017) Modal Analysis of Fluid Flows: An Overview, *AiAA Journal*, **55,** 4013. https://doi.org/10.2514/1.J056060

[16] .Schmid, P.J. (2010)Dynamic Mode Decomposition of Numerical and Experimental Data, *Journal of fluid mechanics*, **656**, 5. https://doi.org/10.1017/S0022112010001217

[17] Hemati, M. S., Rowley, C. W., Deem, E. A., Cattafesta, L. N. (2017) De-biasing the Dynamic Mode Decomposition for Applied Koopman Spectral Analysis of Noisy Datasets, *Theoretical and Computational Fluid Dynamics*, **31**, 349. https://doi.org/10.1007/s00162-017-0432-2

[18] Bogey, C. (2018) Grid sensitivity of flow field and noise of high-reynolds-number jets computed by large-eddy simulation, *International Journal of Aeroacoustics*, **17**, 399. https://doi.org/10.1177/1475472X18778287

[19] Sirovich, L. (1987) Turbulence and the Dynamics of Coherent Structures. i - Coherent Structures. ii - Symmetries and Transformations. iii - Dynamics and Scaling, *Quarterly of Applied Mathematics*, **45**, 561-571. https://doi.org/10.1090/qam/910462

[20] Jovanovic, M.R., Schmid, P.J., Nichols, J. W. (2014) Sparsity-promoting Dynamic Mode Decomposition, *Physics of Fluids*, **26**, 024103. https://doi.org/10.1063/1.4863670

[21] Ho, C.-M., Huerre, P. (1984) Perturbed Free Shear Layers, *Annual review of fluid mechanics*, **16**, 365. https://doi.org/10.1146/annurev.fl.16.010184.002053

[22] Michalke, A. (1972) The Instability of Free Shear Layers, *Progress in Aerospace Sciences*, **12**, 213. https://doi.org/10.1016/0376-0421(72)90005-X

[23] Gutmark, E., Ho, C.-M. (1983) Preferred Modes and the Spreading Rates of Jets, *Physics of Fluids*, **26**, 2932-2938. https://doi.org/10.1063/1.864058

[24] Kinsler, L.E., Frey, A.R., Coppens, A.D., Sanders, J.V. (2000) Fundamentals of Acoustics - 4th Edition, *Wiley*, 283-284.

Nomenclature

c_0 speed of sound in ambient air
D diameter of the jet exit
k_j wavenumber in the jet flow direction
k_k wavenumber in the radial direction
k_l wavenumber in time
K modulus of the air
M Mach number
p_0 ambient pressure
p pressure
p_i pressure at a specific point
p_{ref} sound pressure of the reflected wave
p_t sound pressure of the transmitted wave
r_0 radius of the jet
r displacement in the radial direction
Re Reynolds number
St_D diameter-based Strouhal number
St_θ momentum thickness-based Strouhal number
t time
T_0 ambient temperature
U_j center of the jet velocity
u' fluctuation velocity
$\bar{u}$ time-averaged velocity
u_i velocity of particles
u_{ref} velocity of the reflected wave
u_t velocity of the transmitted wave
u_z flow velocity in the jet flow direction
$u_{r.}$ flow velocity in the radial direction
z displacement of the jet flow direction
z_1, z_2 acoustic impedance of the media
z_l local acoustic impedance
α amplitude of the DMD mode
γ heat capacity ratio
δ_{BL} thickness of the Blasius boundary layer
δt nondimensional time step
ν kinetic viscosity
θ angle in the azimuthal direction
ρ density
ρ_i density at a specific point

σ growth rate of the DMD mode